Sonic Boom Pressure Signature Uncertainty Calculation and Propagation to Ground Noise (Invited)

Thomas K. West IV*
Missouri University of Science and Technology, Rolla, MO 65409
Kathrine N. Bretl†
Massachusetts Institute of Technology, Cambridge, MA 02139
Eric L. Walker‡ and Jeremy T. Pinier§
NASA Langley Research Center, Hampton, VA 23681

The objective of this study was to outline an approach for the quantification of uncertainty in sonic boom measurements and to investigate the effect of various near-field uncertainty representation approaches on ground noise predictions. These approaches included a symmetric versus asymmetric uncertainty band representation and a dispersion technique based on a partial sum Fourier series that allows for the inclusion of random error sources in the uncertainty. The near-field uncertainty was propagated to the ground level, along with additional uncertainty in the propagation modeling. Estimates of perceived loudness were obtained for the various types of uncertainty representation in the near-field. Analyses were performed on three configurations of interest to the sonic boom community: the SEEB-ALR, the 69^o Delta Wing, and the LM 1021-01. Results showed that representation of the near-field uncertainty plays a key role in ground noise predictions. Using a Fourier series based dispersion approach can double the amount of uncertainty in the ground noise compared to a pure bias representation. Compared to previous computational fluid dynamics results, uncertainty in ground noise predictions were greater when considering the near-field experimental uncertainty.

Nomenclature

n	= Number of Positions	U	= Uncertainty Magnitude
X_{Ram}	= Actuator Position	u^-	= Lower Uncertainty Bound
X_{Orif}	= Pressure Port Location	u^+	= Upper Uncertainty Bound
$X_{Aligned}$	= $X_{Orif} + X_{Ram}$	Δu^-	= Lower Uncertainty Increment
$\bar{\bar{f}}$	= Grand Averaged Signature	Δu^+	= Upper Uncertainty Increment
$\bar{f}$	= Temporally Averaged Signature	U	= Uncertainty Magnitude
M	= Mach Number	P	= Pressure
h	= Signature Height	ϵ	= Uncertainty Factor
σ	= Standard Deviation	N	= Partial Fourier Series Order
L_b	= Bias Limit	a_k, b_k, h_k	= Fourier Expansion Coefficients
g_i	= Dispersion Function	Δx	= Phase Uncertainty

*Graduate Student, Department of Mechanical and Aerospace Engineering, Student Member AIAA.
†Undergraduate Student, Department of Aeronautics and Astronautics, Student Member AIAA.
‡Research Aerospace Engineer, Configuration Aerodynamics Branch, Associate Fellow AIAA.
§Research Aerospace Engineer, Configuration Aerodynamics Branch, Senior Member AIAA.

I. Introduction

Sonic boom mitigation has been a critical challenge in the commercializing of supersonic flight. Several low-boom aircraft have been proposed since the original design programs were launched in an effort to overcome the obstacle that over-land flight restrictions pose to the pioneering idea of commercial supersonic flight. Supplementary to this research, there has been ongoing effort in recent years to understand and assess the performance of computational fluid dynamics (CFD) for boom prediction while also identifying the most robust test techniques to capture the pressure signatures of sonic booms from various configurations of aircraft and other bodies. These methods are fashioned to better inform the design of supersonic vehicles.

The primary objective of this study hinges on a better understanding of accuracy requirements for testing techniques, specifically focusing on various methods of uncertainty representation. A better apprehension of the consequences of uncertainty in the sonic boom signatures was pivotal in understanding the impact to the perceived noise of an observer on the ground, which came to be a fundamental aim of this study. The agenda of this study was four-fold: 1) to detail a new approach to quantifying the spatial and temporal uncertainty in sonic boom measurements, 2) to determine the extent to which perceived noise levels vary with changes in the representation of uncertainty, 3) to then apply the various uncertainty representation methods to multiple bodies in order to advise the experimental technique if the variation levels are unacceptable, and 4) to make comparisons of experimental and computational methods to further assess the validity of certification predication passage when considering limitations on ground noise. Previous work by West et al.[1] outlined an approach for estimating certification potential, under uncertainty, of supersonic configurations.

Wind tunnel data from three geometries were chosen for analysis and comparison: the Lockheed-Martin SEEB-ALR, the NASA 69^o Delta Wing, and the Lockheed Martin (LM) 1021-01 low boom-aircraft configuration. Next, the individual data sets were randomly dispersed using a Monte Carlo simulation. Finally, the sonic boom signatures for each of the cases were propagated to the ground and the resultant perceived loudness level calculations were computed. Once the ground propagations were integrated, an additional step was to isolate the effect of each uncertainty representation on the perceived ground noise variation to compare methods.

The following section further describes the experimental testing procedure and the uncertainty estimation procedure for the experimental measurements. Section III details the uncertainty interval measurement and dispersion methodologies. Section IV then briefly describes the sonic boom propagation to the ground level and the associated sources of uncertainty. Finally, Section V outlines the results of the study and Section VI summarizes the important findings of this work.

II. Experimental Measurements and Uncertainty Estimation

In this section, the experimental setup for measuring near-field sonic boom signatures is detailed, along with the three sonic boom configurations investigated in this study. Lastly, the spatial averaging technique used to quantify the near-field uncertainty is discussed in detail.

A. Experimental Setup

In October 2011 and October 2012, experiments were conducted at the NASA Ames 9 x 7 Foot Supersonic Wind Tunnel to measure near-field sonic boom pressure signatures at Mach 1.6 and 1.7 and a unit Reynolds number of approximately $4.3\text{x}10^6$ per foot. Sonic booms generated by tested configurations were measured using a nominally invasive Reflection Factor 1 (RF1) pressure rail, which contained 420 pressure ports spaced approximately 4 mm apart. Configurations were placed on a linear actuator within the tunnel and the model was translated either in the X direction (into the flow) or in the Z-direction (away from the pressure rail) and measurements were taken during sweeps of the model. Further detail regarding the experimental testing is given by Cliff et al.[2]

The three geometries used in this study are shown in Figure 1. The SEEB-ALR model (left) is recognized by a flat-top signature, leaving flow-field variations easy to identify. It is further described by Morgenstern et al.[3] The 69^o Delta Wing features a 69^o leading edge sweep angle, and is a modification of the 59^o body. This modification further reduced maximum overpressure significantly, by lengthening the lift-load model distribution. Further discussion of the 69^o Delta Wing configuration is found in Hunton et al.[4] The final geometry of the study is the Lockheed Martin 1021-01 low boom configuration, designed based on predictions

of low boom. Ultimately, it boasts a smooth rather than sharp pressure signature. This configuration is further detailed by Morgenstern et al.[5]

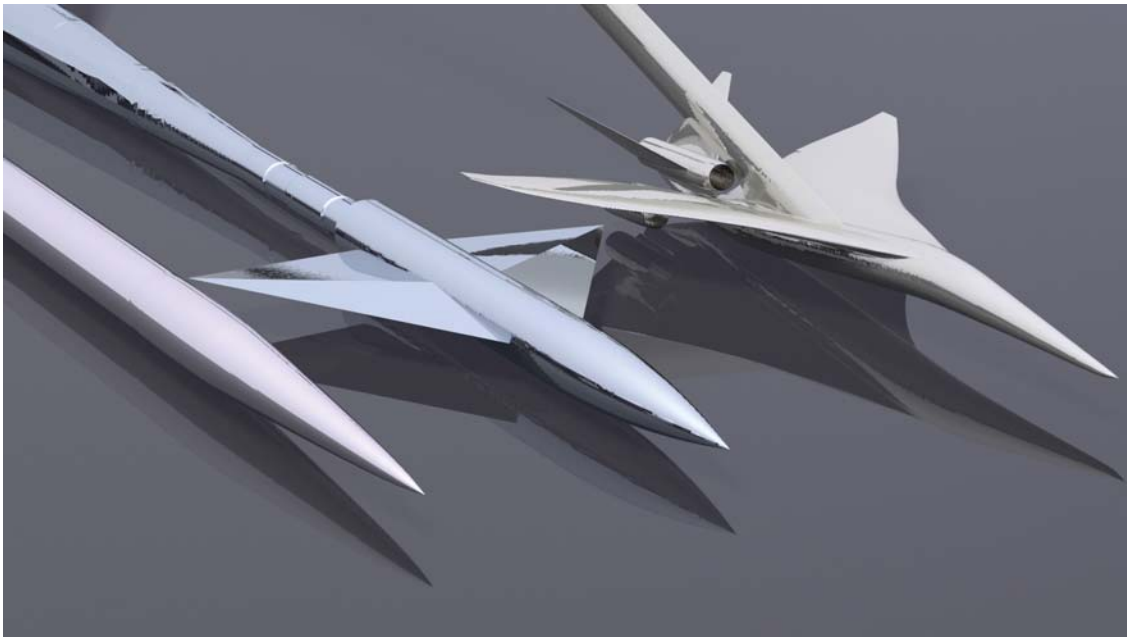

Figure 1: Configurations studied in the present work. SEEB-ALR (left), NASA 69° Delta Wing (center), LM 1020-01 (right). Models not to relative scale. (Aftosmis et al.[6])

B. Uncertainty Estimation

A spatial averaging technique was developed to reduce the effect of tunnel flow field spatial distortions on the data at single model positions during supersonic wind tunnel testing. Sonic boom testing in the 9x7 wind tunnel has shown that the expected non-uniform flow field causes pressure signatures on the rail to be different for different model positions in the test section. To enable the spatial averaging technique, the model is typically translated a short distance horizontally or vertically, and a number of sonic boom signatures are acquired at multiple positions and averaged. The reported linear actuator position, $X_{_{Ram}}$, is added to axially shift the pressure signature data to align each series of pressures so that simple averaging of the data could be accomplished. Simply stated, the grand averaged signature $\bar{\bar{f}}(x)$, is obtained by summing individual temporally averaged signatures, $\bar{f}_i(X_{_{Orif}})$, at each port $X_{_{Orif}}$ and dividing by n, the number of positions.

$$\bar{\bar{f}}(x) = \frac{\sum_{i=1}^{n} \bar{f}_i(X_{_{Aligned}})}{n} \tag{1}$$

where,

$$X_{_{Aligned}} = X_{_{Orif}} + X_{_{Ram}} \tag{2}$$

$$\bar{f}(X_{_{Orif}}) = \frac{\sum_{j=1}^{k_1} f_{ij}(X_{_{Orif}})}{k_1} - \bar{f}_{_{Ref}}(X_{_{Orif}}) \tag{3}$$

$$\bar{f}_{_{Ref}}(X_{_{Orif}}) = \frac{\sum_{j=1}^{k_2} f_{0j}(X_{_{Orif}})}{k_2} \tag{4}$$

Here, i is the counter for the Ram positions, j is the counter for data point samples, $\bar{f}_i$ is the ith temporal average at rail position X_{Orif}, $\bar{f}_{Ref}$ is the temporal average of reference signatures f_{0j}, and k_1, k_2 are the intervals of the temporal average for the data run signatures, f_i, and reference run signatures, f_{Ref}, respectively.

Theoretically, the mean signature is obtained at each port where the shifted signatures align perfectly. In practice, interpolation is required between the port measurements on the rail to properly align the signatures with minimal setpoint error. Figure 2(a) is a sample set of measurements taken for the LM 1021-01 during a sweep in the X direction (into the flow). Figure 2(b) shows aligned pressure signatures for the run series; the result of adding the linear actuator position X_{Ram} to each pressure signature. The blue colored pressure signature at the bottom of the plot is the mean or averaged pressure signature of the run series. Note that this type of figure is referred to as a waterfall plot.

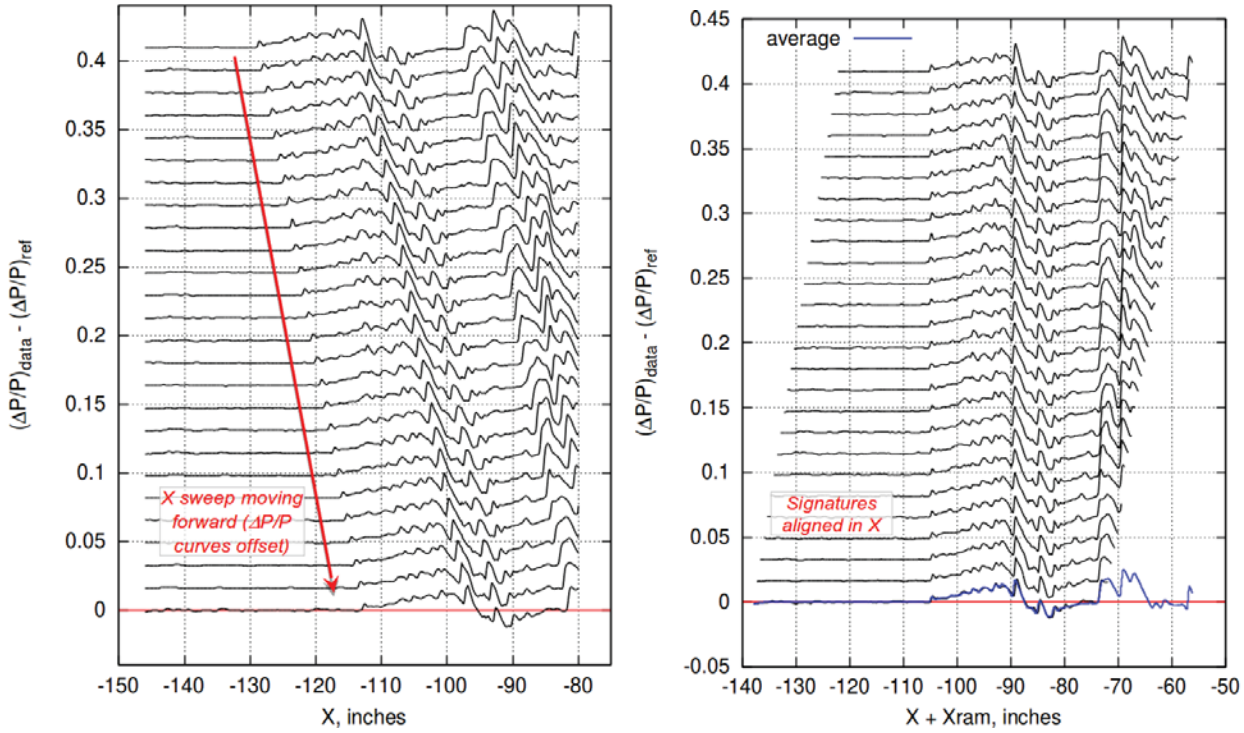

(a) Non-aligned (b) Aligned

Figure 2: Sample waterfall plots of the LM 1021-01 during an axial sweep, M = 1.6, h = 31.33. (Cliff et al.[2])

To begin estimation of uncertainties for the spatial averaging technique, it is necessary to compute several components of variation from the test data. For the purpose of understanding the behavior of the test techniques, a relative uncertainty analysis is performed. This analysis is useful for the comparison of spatially averaged signatures and is not necessarily indicative of the total uncertainty of the final averaged signature.

Using the method described by Walker[7] for developing a dispersion relationship for equations with multiple levels of variation, the dispersion σ^2 of the grand averaged signature $\bar{\bar{f}}(x)$ can be written as

$$\sigma^2_{\bar{\bar{f}}(x)} = \frac{\sum_{i=1}^{n}\left[\sigma^2_{sp} + \sigma^2_{\bar{f}_i(X_{Orif})} + \sigma^2_{\bar{f}_{ref}(X_{Orif})}\right]}{n} \tag{5}$$

where,

$$\sigma^2_{sp} = \sigma^2_{ar} - \sigma^2_{\bar{f}_i(X_{Orif})} \tag{6}$$

$$\sigma^2_{ar} = \frac{1}{n}\sum_{i=1}^{n}[\bar{f}_i(X_{Orif}) - \bar{\bar{f}}(x)]^2 \tag{7}$$

Here, σ^2_{sp} is the spatial standard deviation of the ith model position at rail position X_{Orif}, $\sigma^2_{\bar{f}_i(X_{Orif})}$ is the temporal standard deviation of the ith model position at rail position X_{Orif}, $\sigma^2_{\bar{f}_{Ref}(X_{Orif})}$ is the temporal standard deviation of the reference run at rail position X_{Orif}, and σ^2_{ar} is the spatial standard deviation across runs of the ith model position at rail position X_{Orif}.

The reported uncertainty band applied to the grand mean sonic boom pressure signature is $\pm 2\sigma^2_{\bar{\bar{f}}(x)}$. Because the primary application of the uncertainty band was to compare signatures, no fossilized uncertainty was included in the uncertainty buildup. Some of the fossilized uncertainty due primarily to calibration of the pressure measurement devices may also be mitigated by subtraction of the reference signatures. At best, the uncertainty bands or intervals provided should be deemed to represent a minimum level of uncertainty for the purpose of signature comparison. The interval is set to a width of four standard deviations with no statement of the associated distribution. This corresponds to 95% coverage for a normal distribution. However, given the low sample sizes for the experimental data it is best to not assume or imply a distribution.

III. Boom Dispersions

The uncertainty interval calculation approach given in the previous section is used to determine the symmetric interval about the averaged sonic boom signature. There are two issues with using this interval for a ground noise uncertainty analysis. The first is that the interval calculated is symmetric throughout a signature. Sonic boom pressure signatures inherently have large gradients, which may make a symmetric uncertainty band under-represent the uncertainty in high gradient regions. This can be addressed by accounting for the local gradient and adjusting the uncertainty band accordingly using an asymmetric uncertainty approach, as purposed by Pinier.[8]

The second issue is related to the propagation of the near-field uncertainty to ground noise, which is the main goal of this study. However, the calculated uncertainty interval does not provide an indication as to the behavior of the signature within the uncertainty band other than the shape of the averaged signature, which is uncertain as well. The uncertainty in the sonic boom signature is different than traditional single point uncertainty measurements. Sonic booms have a distributed uncertainty with a spatial correlation between the signature and the vehicle. Therefore, a single point analysis with a bias uncertainty may not be sufficient in this type of uncertainty analysis. To overcome this, a dispersion model must be implemented to generate random signature shapes within the bounds of the uncertainty, and propagate the dispersion to the ground level. The remainder of this section compares the symmetric versus asymmetric uncertainty representation approach and the sonic boom dispersion model.

A. Symmetric vs. Asymmetric Uncertainty

In the context of sonic boom signatures, uncertainty is added and/or subtracted from the nominal signature in order to form an uncertainty band. The upper and lower uncertainty bounds are given in Eqs. (8) and (9), respectively.

$$u^+(x) = \frac{\Delta P}{P}(x) + \Delta u^+ \tag{8}$$

$$u^-(x) = \frac{\Delta P}{P}(x) - \Delta u^- \tag{9}$$

Here, Δu^+ is the positive uncertainty and Δu^- is the negative uncertainty. In traditional bias representation with symmetric uncertainty, the lower and upper bounds of the uncertainty are the same, as shown in Eq. (10), and is only based on the measurement accuracy.

$$\Delta u^+ = \Delta u^- = U \tag{10}$$

While a symmetric representation may be adequate for a single point measurement, it is not likely to be the sole mechanism required to represent deficiencies in the measured signatures. Because there are not perfect correlations of all of the individual pressures that make up a boom signature, an additional uncertainty method is required to account for these imperfections.

Asymmetric uncertainty provides an uncertainty calculation based on the gradients present in the boom signature.[8] A prescribed amount of spatial uncertainty is propagated through the signature such that the

$\Delta P/P$ measurement uncertainty is inflated proportional to the local gradient of the pressure signature at any given point. Rather than being concerned with simply the pressure component of the signature, the spatial uncertainty accounts for error in location as well. Eqs. (11) and (12) define the upper and lower magnitudes of asymmetric uncertainty, respectively.

$$\Delta u^{+}(x) = U + \left| \frac{\Delta P}{P}(x) - \frac{\Delta P}{P}(x + \Delta x \; sgn\left(\frac{d(\frac{\Delta P}{P})}{dx}\right)) \right| \tag{11}$$

$$\Delta u^{-}(x) = U + \left| \frac{\Delta P}{P}(x) - \frac{\Delta P}{P}(x - \Delta x \; sgn\left(\frac{d(\frac{\Delta P}{P})}{dx}\right)) \right| \tag{12}$$

Here, U is the previously calculated bias or symmetric uncertainty and Δx is the phase uncertainty in the input. In this study, Δx is assumed to be 1/16 of an inch, which is just under half of the spacing between the ports on the pressure rail. This model allows for the propagation of phase-uncertainty in location. If the gradient of the nominal function is positive, the upper uncertainty increment will increase, and the lower uncertainty increment will spike just following that of the upper uncertainty. This almost simultaneous jump in both directions creates an increase in the width of the uncertainty band, adding a phase-uncertainty at the location of the large gradient.

Figures 3(a), 4(a), and 5(a) show the pressure signatures of the three configurations of interest. Included in these figures are the symmetric and asymmetric uncertainty bands. For better visualization, figures 3(b), 4(b), and 5(b) show the uncertainty bands with the nominal signature subtracted off to show a residual scale of the signatures. Notice that in comparing the asymmetric to the symmetric uncertainty bands, the largest difference exists in the high gradient regions of the signature. This is the expected outcome given that the asymmetric approach is geared towards the treatment of these regions in the signatures.

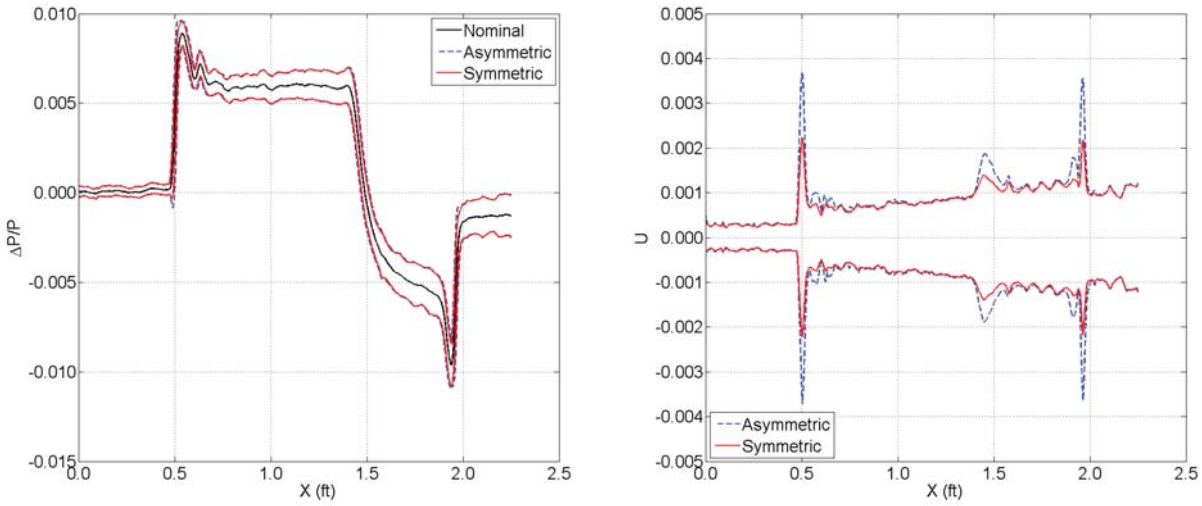

(a) Signatures

(b) Residual Scale

Figure 3: SEEB-ALR near-field pressure signature with asymmetric and symmetric uncertainty.

The difference between the asymmetric and symmetric uncertainty approaches can be quantified by determining the area within the two intervals. A summary of the areas for all three configurations is given in Table 1. There is a significant effect of the asymmetric uncertainty treatment. For example, the area of the uncertainty band for the LM 1021-01 is more than 30% larger than the band for the symmetric uncertainty treatment. Later in this study, a comparison of the effect on ground noise for symmetric versus asymmetric uncertainty representation is investigated.

The spatial averaging technique in conjunction with other aspects of model testing can cause rounding of the peaks in the boom signatures,[2] thus reducing the sharpness of the peaks in the signature and creating

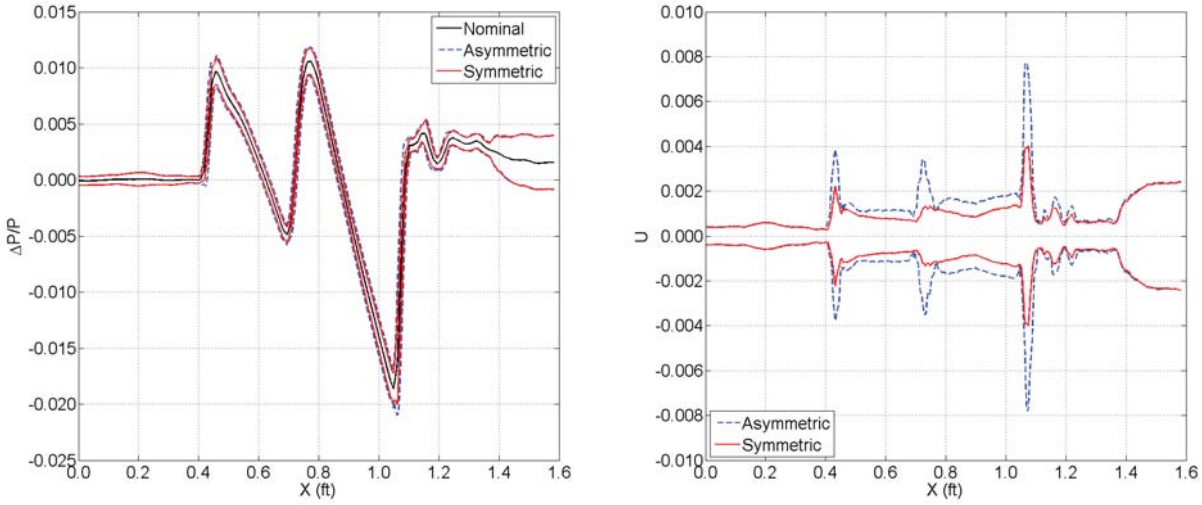

(a) Signatures (b) Residual Scale

Figure 4: 69^o Delta Wing near-field pressure signature with asymmetric and symmetric uncertainty.

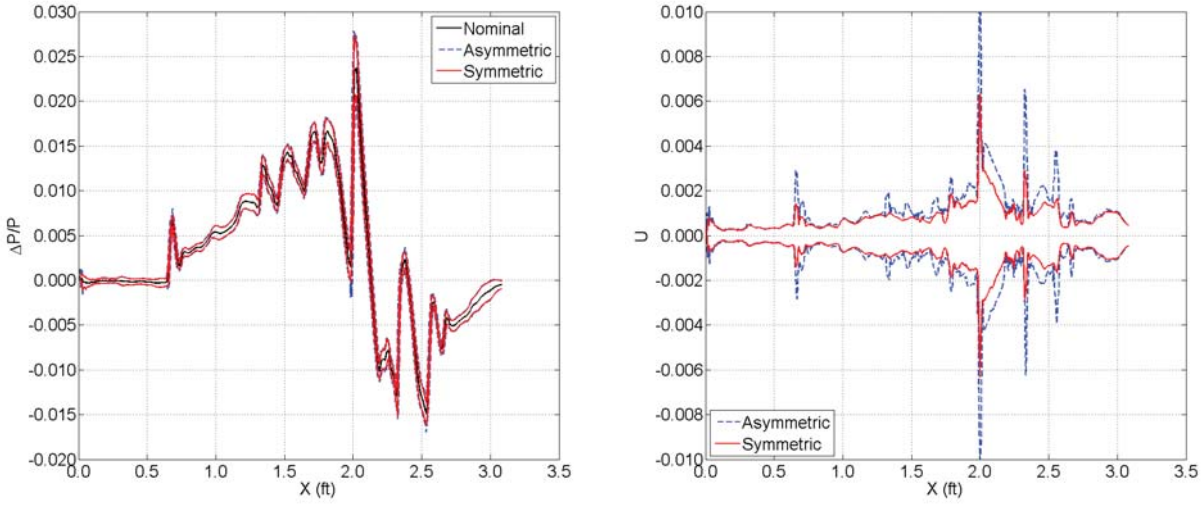

(a) Signatures (b) Residual Scale

Figure 5: LM 1021-01 near-field pressure signature with asymmetric and symmetric uncertainty.

a false sense of boom dampening. As this rounding is a known source of error, the use of the asymmetric approach may help to widen the uncertainty at the peaks.

B. Fourier Dispersion

After determining the uncertainty band around the nominal signature, as detailed above, the next step is to sample possible signatures within the band. Sonic boom loudness metrics depend on the shape of the signature, especially in the regions of shocks and expansions. Pinier[9] described an approach for generating random dispersions within specified boundaries. The dispersed function, $\tilde{f}$ within specified uncertainty bounds is shown in Eq. (13).

Table 1: Uncertainty band area for symmetric and asymmetric uncertainty.

Configuration	Symmetric	Asymmetric	% Difference
SEEB-ALR	3.629×10^{-3}	4.063×10^{-3}	11.29
69^o Delta Wing	3.144×10^{-3}	4.182×10^{-3}	28.31
LM 1021-01	5.249×10^{-3}	7.265×10^{-3}	32.23

$$\tilde{f}(x) = f(x) + \epsilon_i L_b u(x) + (1 - |\epsilon_i L_b|) g(x) u(x) \tag{13}$$

Here, u is the uncertainty, L_b is the bias limit, ϵ_i a randomly sampled uncertainty factor with $-1 \leq \epsilon_i \leq 1$, and g is a partial sum Fourier series given by:

$$g(\bar{x}) = \sum_{k=1}^{N} (a_k sin(2\pi(k\bar{x} + h_k)) + b_k cos(2\pi(k\bar{x} + h_k))) \tag{14}$$

where a_k, b_k, and h_k are randomly generated real numbers uniformly distributed between -1 and 1, and $\bar{x}$ varies on a normalized scale from 0 to 1. N is the order of the partial Fourier series. Note that the random phase, h_k, allows for the uncertainty band to be fully covered by the dispersion function.

The bias limit, L_b is used to control the amount of uncertainty that comes from systematic errors and randomized error sources. A bias limit of one assumes that all of the uncertainty is systematic and is therefore modeled as simple bias. Pinier[9] states that this is unrealistic for most cases. On the other hand, Pinier[9] states a bias limit of zero may be justifiable given a strong physical argument. Figures 6(a) and 6(b) show examples of how the dispersions are different for a bias limit of one and zero, respectively. Note that these signatures are in the residual scale (i.e., the averaged signature is subtracted off). Notice that with the bias limit set to one, the dispersed signatures closely follow the shape of the baseline signature. However, with the bias limit at zero, the dispersions appear much more random. Later in this study, the effect of the bias limit on ground noise prediction is investigated.

This dispersion model was originally introduced to realistically represent random variations in flight simulations using traditional uncertainty bounds. However, this approach is highly applicable to the asymmetric uncertainty method described above, which accounts for the original lack of inclusion of phase errors. It most notably allows for the rotation of the signature within the uncertainty bounds. Local sharpening of the peaks of the signatures may be observed, which directly affects the ground noise. This particular feature of this dispersion model helps to improve the rounding of the signature peaks observed in the experimental measurement results.[2]

In order to apply this dispersion approach, the order of the Fourier series must be determined. A spectral analysis, using a fast Fourier transform (FFT) of the nominal signature, can highlight those frequencies that carry the most energy in the signature. Relative magnitude versus frequency plots for the three configurations are given in Figures 7(a), 7(b), and 7(c). These figures only show the first 50 frequencies as all higher frequencies have a near zero magnitude. These figures also show a spectral analysis of the baseline CFD signatures obtained by West et al.[1] This was performed to show that the CFD signature exhibit nearly the same frequency content as the experimental signature.

Table 2 shows the top three frequencies for each of the three configurations investigated in this study. Note that these frequencies are ordered from highest to lowest. While these frequencies have been identified to carry significant information, what is unknown is how many of these frequencies directly influence ground noise predictions. The objective in this study will be to incrementally add frequency content to the dispersion until the ground noise prediction uncertainty is unchanged.

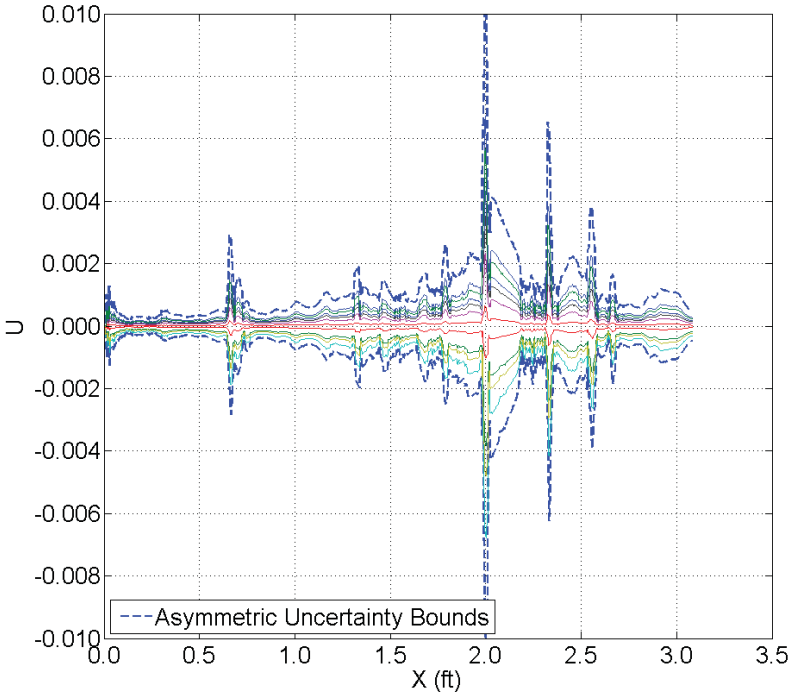

(a) Bias Limit of 1

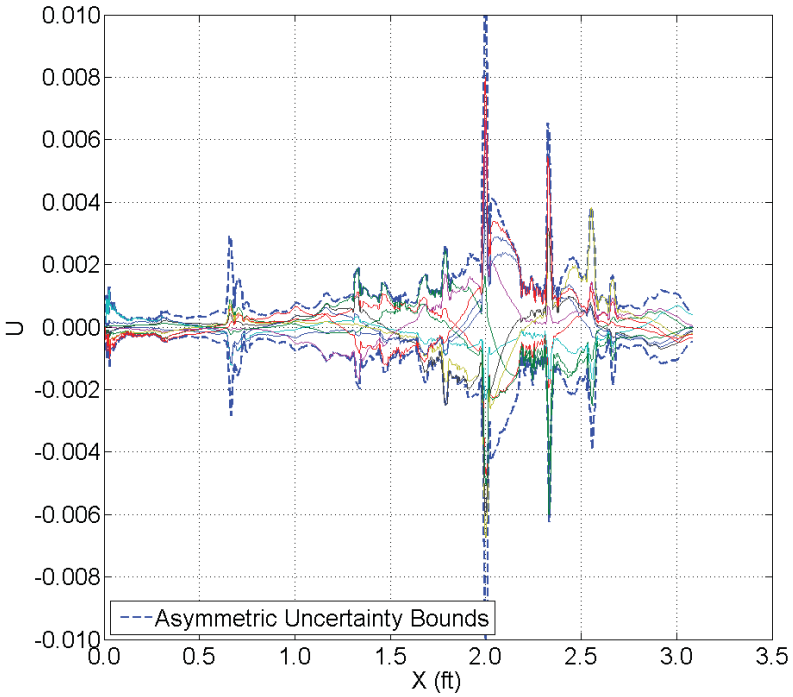

(b) Bias Limit of 0

Figure 6: LM 1021-01 near-field dispersions.

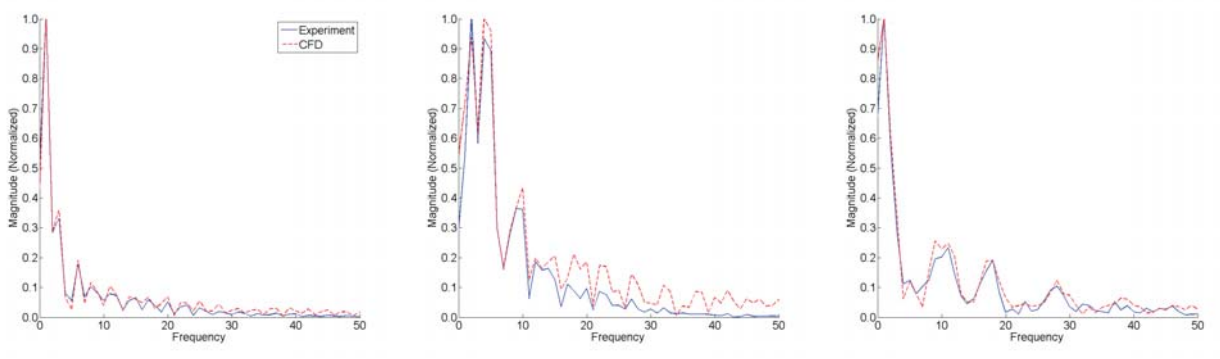

(a) SEEB-ALR (b) 69^o Delta Wing (c) LM 1021-01

Figure 7: Magnitude vs. frequency plot baseline experimental and CFD signatures.

Table 2: Key frequencies of each nominal sonic boom signature.

Configuration	Frequencies
SEEB-ALR	1,3,2
69^o Delta Wing	2,4,5
LM 1021-01	1,2,3

IV. Sonic Boom Propagation to Ground Noise

After quantifying the near-field uncertainty, the next step is to propagate that uncertainty to the ground level. This section will briefly discuss the propagation of a sonic boom to the ground level. Additionally, uncertainty in the propagation is identified and is used in the overall uncertainty analysis, in tandem with near-field uncertainty.

A. Boom Propagation Approach

After implementing various uncertainty methods, the set of signatures needs to be evaluated for their respective perceived ground noise levels. Accomplishing this analysis requires two main steps, the first of which was to propagate the signature to the ground using a program called sBOOM. This model uses an augmented Burger's equation to propagate the near-field pressure signature to the ground level. The model takes into account nonlinear effects, thermoviscous absorption, atmospheric stratification, spreading, and many other molecular relaxation phenomena. Further details regarding this model are given by Rallabhandi.[10] The second step is to integrate the signature to find the perceived ground noise and calculate the level of perceived loudness (PLdB).

B. Boom Propagation Uncertainty

In addition to the uncertainty in the near-field pressure signature measurements, uncertainty may also exist in the propagation of the sonic boom to the ground level. West et al.[1] identified key sources of both epistemic and aleatory uncertainty through an uncertainty and sensitivity analysis of the computational fluid dynamics models of the configurations of interest in the present study. Based on the previous work, the top four uncertain parameters have been selected to be used as part of the uncertainty analysis in the current work. The aleatory uncertainty parameters, their distributions, and uncertainty ranges are given in Table 3. Epistemic parameters and their interval bounds are given in Table 4. Note that these four parameters account for about 99% of the previously considered uncertainty in the propagation modeling.

Table 3: sBOOM aleatory uncertain parameters.

Input	Distribution	Mean	Std. Dev.
Temperature Profile (%)	Gaussian	1.0	0.01
Humidity Profile (%)	Gaussian	1.0	0.01

Table 4: sBOOM epistemic uncertain parameters.

Input	Lower Bound	Upper Bound
Reflection Factor	1.8	2.0
Ground Elevation (ft)	0.0	5000.0

C. Uncertainty Analysis

With the uncertainty representation approach and sources of uncertainty outlined in the previous sections, the last step is to propagate the uncertainty to ground noise. This is done by using a Direct Simulation Monte Carlo (DSMC). This requires rigorous evaluation of the deterministic model (Fourier dispersion coupled with the sBoom propagation code), which is not overly computationally expensive. Note that a convergence study was performed, which showed that a total of 10,000 samples were required to converge the Monte Carlo simulations.

Recall from the previous sections that sources of uncertainty include the uncertainty in the near-field pressure signature measurements and the uncertainty in the propagation. The number of uncertain parameters depends on the order of the Fourier sum as each frequency included will have three random parameters, namely a_k, b_k, and h_k. Again, these parameters are uniformly distributed and are considered aleatory sources of uncertainty. Note that the computational expense of a Monte Carlo simulation is independent of the number of uncertain parameters. Because the uncertainty in the propagation is of both epistemic and aleatory types, proper treatment when propagating the uncertainty is necessary for accurate representation of the output uncertainty.

In this study, the second-order probability approach described by Eldred and Swiler[11] is employed to propagate mixed uncertainty. This approach is a type of double loop sampling where the outer loop contains the epistemic samples, which are passed into the inner loop where the deterministic model is sampled for every aleatory sample vector. Each iteration of the outer loop generates a cumulative distribution function (CDF) based on the aleatory uncertainty analysis in the inner loop. After completion of the process, what remains is a series of CDFs, which, when plotted, gives intervals of the output variable from the model at different probability levels (i.e., a probability or "P-box" representation of mixed uncertainty output). Important information can be taken from P-boxes, including confidence intervals. For the case of mixed uncertainty, one approach to obtaining the 95% confidence interval, for example, is to take the upper 97.5% probability level and the lower 2.5% probability level as the interval. The P-box and confidence interval measurement are illustrated in Figure 8.

V. Results

Section III described multiple approaches for representing the near-field uncertainty. However, the effect that each of these approaches has on the ground noise uncertainty prediction is yet to be determined. First, the influence of the asymmetric uncertainty representation over the symmetric approach needs to be investigated. This was done using Eq. (13) with the bias limit, $L_b = 1$ and $g(x) = 0$, which represents a full bias dispersion without the use of the Fourier dispersion approach. Note that this isolates the effect of the asymmetric versus symmetric representation. The only uncertainty then is what is present in the propagation modeling, which was kept the same for each of the scenarios.

Results indicated that there was an insignificant difference in the loudness predictions between the asymmetric and symmetric cases. This is the result of the selected Δx value used in the asymmetric analysis

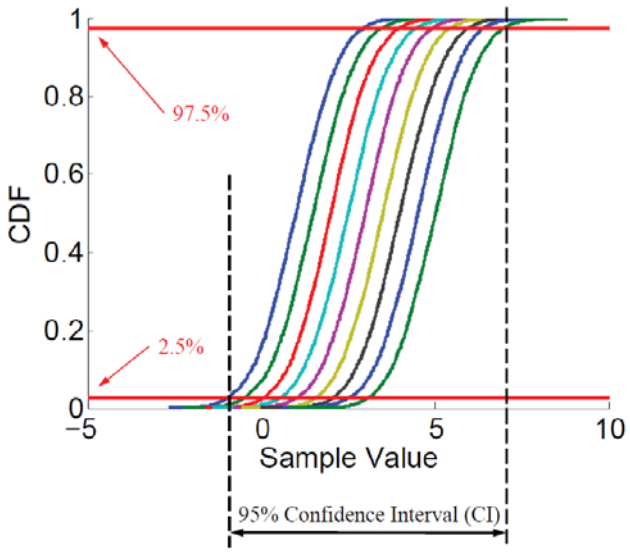

Figure 8: P-box representation of mixed uncertainty output and confidence interval measurement.

(see section III). However, an important analysis can be made using this pure bias uncertainty information. Figure 9 shows a comparison of the bias only, asymmetric P-boxes versus those obtained for the CFD simulations.[1] Notice that, in general, the slopes of the P-boxes are relatively similar compared to the CFD, for each configuration. Also, note that the loudness values being larger for the CFD analysis is expected due to the peak rounding in the experimental data, which directly effects loudness predictions.[1,2] This will be addressed with the Fourier dispersion method.

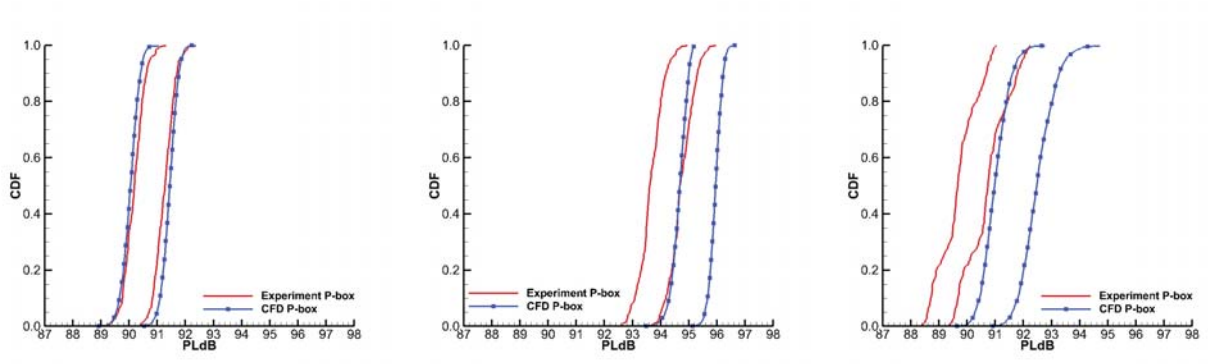

(a) SEEB-ALR (b) 69^o Delta Wing (c) LM 1021-01

Figure 9: P-boxes of PLdB with CFD comparison for asymmetric bias uncertainty only.

Using the asymmetric uncertainty band approach, the next step was to add in the effect of the Fourier dispersions. For each of the three configurations of interest, the order of the partial Fourier series given in Eq. (14) must be determined. This is done by adding frequency content to the partial Fourier sum until convergence of the 95% confidence interval in the ground noise metric PLdB was observed. Convergence was achieved when each of the 95% confidence interval limits changed by less than 0.1 PLdB. Note the frequencies were added in order of their magnitudes, starting with the largest.

The convergence of the 95% confidence intervals of PLdB versus the number of frequencies are shown in Figure 10 for the three configurations. For the SEEB-ALR, the content from the top nine frequencies, in terms of magnitude, was required for convergence. These frequencies account for about 70% of the total energy in the signature. The frequency content of the top five frequencies, was required for the 69^o Delta Wing. These frequencies account for about 50% of the total energy in the signature. Lastly, for the LM 1021-01, the top nine frequencies were required. These frequencies also account for about 50% of the total

energy in the signature.

For the 69^o Delta Wing and the LM 1021-01, an interesting result is that only about half of the frequency content of the near-field signature is required to converge the ground noise uncertainty prediction. This is likely due to the fact that higher frequencies have relatively small magnitudes and each of these higher frequencies weakly contributes to the energy of the signature. Also, because of the small magnitude, the content that these higher frequencies add to the signature is likely damped out when the sonic boom is propagated to the ground. However, the SEEB-ALR required more energy. This is because the SEEB-ALR possesses a greater amount of high frequency content than the other two configurations. From Table 2, these three frequencies only account for about 50% of the energy. This indicates that there may be a lot of higher frequency content, which may influence the shape of the signature more significantly. For all of the configurations only the first three frequencies were necessary to obtain a relatively accurate prediction. Additional frequencies were required, however, to meet the tight convergence requirement.

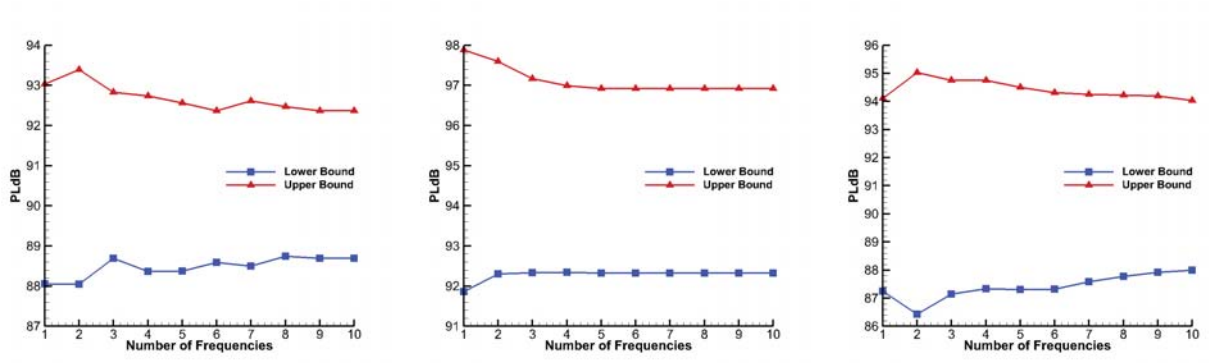

(a) SEEB-ALR (b) 69^o Delta Wing (c) LM 1021-01

Figure 10: 95% confidence interval convergence.

Note that these results were obtained using a bias limit, L_b of zero. The above analysis was repeated with a bias limit of one in order to quantify the effect of modeling the uncertainty as systematic or random. For the LM 1021-01, the 95% confidence intervals for $L_b = 0$ and $L_b = 1$ are [87.99 , 94.03] and [88.45 , 93.63], respectively. Notice that the interval for $L_b = 0$ (i.e., all of the uncertainty is due to randomized sources) is about 0.9 PLdB wider. This result is expected as the bias uncertainty restricts the shape of the dispersion to the shape of nominal signature. Also, the more random signatures observed for the $L_b = 0$ case may allow for more local sharpening of peaks, which can directly affect the loudness. For design purposes, the more conservative approach will be to assume a bias limit of zero. However, future work may be placed in setting a bias limit that is less conservative, based on a better physical understanding of the uncertainty.

There is merit in comparing the uncertainty in the ground noise based on the experiment versus that based on the CFD. West et al.[1] previously investigated the uncertainty associated with the CFD simulations. The P-boxes for the CFD and the converged experimental results are shown in Figure 11 for the three configurations, along with the baseline noise values, which are the loudness values calculated from the signature without the presence of uncertainty. Note that in these figures what is shown are the boundaries of the P-boxes, without the intermediate CDFs (see Figure 8). A comparison of the 95% confidence intervals is given in Table 5. Note that the CFD results reported are those obtained with fully turbulent solutions.

Table 5 shows that experimental ground noise uncertainty bounds the CFD predictions. This suggests that the experimental uncertainty would be greater than the CFD uncertainty. Compared to the P-boxes in Figure 9, the experimental results capture the uncertainty present in the CFD, but significantly deviate from the shape of the CFD results. The upper probability levels overshoot the CFD. As a result, during certification prediction, a margin between the experimental results and an upper limit on the loudness would always be smaller compared to the margin between the CFD results and the same upper loudness limit. This then may imply that current CFD analyses may not account for enough uncertainty. No claim can be made that the CFD is "less uncertain" as there is no way to validate this claim. However, there are also known deficiencies in the experimental measurement of sonic booms. Improvement of measurement capabilities may improve the results and subsequent uncertainty estimations.

When using this information for the purposes of certification of various configurations or in design under

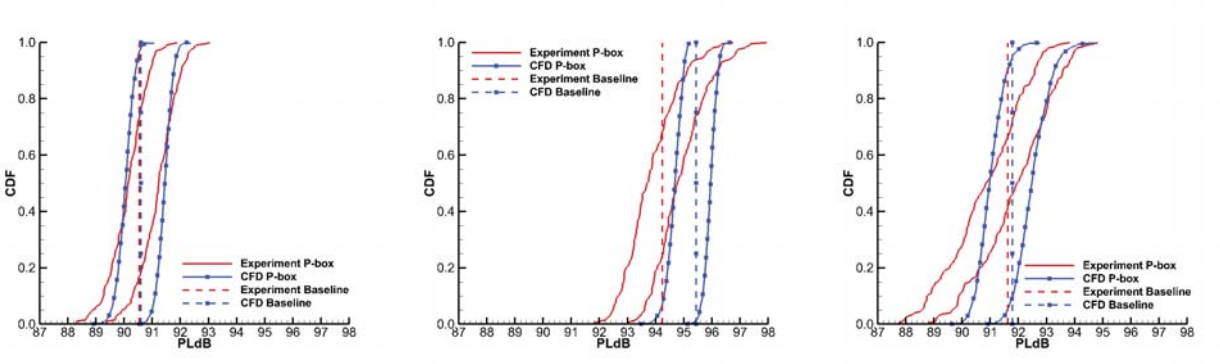

(a) SEEB-ALR (b) 69^o Delta Wing (c) LM 1021-01

Figure 11: P-boxes of PLdB with CFD comparison.

Table 5: 95% confidence intervals of PLdB ground noise prediction.

Configuration	Experiment	CFD[1]
SEEB-ALR	[88.68 , 92.37]	[89.44 , 91.95]
69^o Delta Wing	[92.32 , 96.92]	[94.03 , 96.35]
LM 1021-01	[87.99 , 94.03]	[90.17 , 93.79]

uncertainty, a combination of computation and experimental results should be used in the decision making process to provide the most reliable outcomes. One approach may be to propagate a frequency based dispersion with the CFD in order to capture those uncertainties not observed in the CFD, but are present in the experiment. In other words, the inclusion of model-form uncertainty in the CFD is crucial for an accurate uncertainty analysis. The incorporation of both uncertainty measurements into a certification prediction framework is the subject of future work.

VI. Conclusions

The objective of this study was to outline an approach for the quantification of uncertainty in sonic boom measurements and to investigate the effect of various uncertainty representation approaches on ground noise predictions. The goal was to quantify this by propagating the near-field measurement uncertainty to the ground level to obtain estimations of ground noise uncertainty, along with additional uncertainty in the propagation modeling. Analyses were carried out on three configurations of interest to the sonic boom community: the SEEB-ALR, the 69^o Delta Wing, and the LM 1021-01.

Results showed that, in general, ground noise predictions were sensitive to how the uncertainty was represented in the flow field. Most notably, the effect of using a Fourier dispersion technique within the uncertainty band widened the ground noise uncertainty confidence interval by allowing for local sharpening of peaks that were not captured during the experimental measurements. For the LM 1021-01, the perceived loudness had a 95% confidence interval with about a 6.0 dB width, compared to an interval with only a 3.5 dB width with no Fourier series based dispersion. Similar results were observed for the other two configurations.

Additional comparison was also made between experimental results and previously obtained CFD results. In general, the experimental ground noise uncertainty bounds the CFD predictions. For the purpose of certification prediction, the experimental results may yield a smaller margin with more uncertainty. For an accurate and reliable analysis, a combination of the experimental and CFD uncertainty predictions may be the best approach.

References

[1]West IV, T. K., Reuter, B. W., Walker, E. L., Kleb, B., and Park, M. A., "Uncertainty Quantification and Certification Prediction of Low-Boom Supersonic Aircraft Configurations," *32nd AIAA Applied Aerodynamics Conference*, AIAA 2014-2139, Atlanta, GA, June 2014.

[2]Cliff, S. E., Durston, D. A., Elmiligui, A. A., Jensen, J. C., and Chan, W. M., "Computational and Experimental Assessment of Models for the First AIAA Sonic Boom Prediction Workshop," *52nd AIAA Aerospace Sciences Meeting*, AIAA 2014-0560, National Harbor, MD, Jan. 2014.

[3]Morgenstern, J., Norstrud, N., Sokhey, J., Martens, S., and Alonso, J. J., "Advanced Concept Studies for Supersonic Commercial Transports Entering Service in the 2018 to 2020 Period," NASA CR-2013-217820, NASA Langley Research Center, Feb. 2013.

[4]Hunton, L. W., Hicks, R. M., and Mendoza, J. P., "Some Effects of Wing Planform on Sonic Boom," Tech. rep., NASA TN D-7160, Jan. 1973.

[5]Morgenstern, J. M., Buonanno, M., and Marconi, F., "Full Configuration Low Boom Model and Grids for 2014 Sonic Boom Prediction Workshop," *51st AIAA Aerospace Sciences Meeting*, AIAA 2013-0647, Grapvine, TX, Jan. 2013.

[6]Aftosmis, M. J. and Nemec, M., "Cart3D Simulations for the First AIAA Sonic Boom Prediction Workshop," *52nd AIAA Aerospace Sciences Meeting*, AIAA Paper 2014-0558, Jan. 2014.

[7]Walker, E. L., "Statistical Calibration and Validation of a Homogeneous Ventilated Wall-Interference Correction Method for the National Transonic Facility," Tech. rep., NASA/TP-2005-213947, Dec. 2005.

[8]Pinier, J. T., "Asymmetric Uncertainty Expression for High Gradient Aerodynamics," *50th AIAA Aerospace Sciences Meeting*, AIAA 2012-0081, Nashville, TN, Jan. 2012.

[9]Pinier, J. T., "New Aerodynamic Data Dispersion Method with Application to Launch Vehicle Design," *Journal of Spacecraft and Rockets*, Vol. 49, No. 5, Sept.–Oct. 2012, pp. 834–841.

[10]Rallabhandi, S. K., "Advanced Sonic Boom Prediction Using the Augmented Burgers Equation," *Journal of Aircraft*, Vol. 48, No. 4, July–Aug. 2011, pp. 1245–1253.

[11]Eldred, M. and Swiler, L., "Efficient Algorithms for Mixed Aleatory-Epistemic Uncertainty Quantification with Application to Radiation-Hardened Electronics; Part I: Algorithms and Benchmark Results," Tech. Rep. SAND2009-5805, Sandia National Laboratories, September 2009.